Energy Fuels **2010,** *24,* 581–589 · DOI:10.1021/ef900823s
Published on Web 10/30/2009

energy&fuels
article

Hydrogen Storage in Prussian Blue Analogues: H_2 Interaction with the Metal Found at the Cavity Surface

C. P. Krap,[†] J. Balmaseda,[‡] L. F. del Castillo,[‡] B. Zamora,[†] and E. Reguera*,[†,§]

[†]*Centro de Investigación en Ciencia Aplicada y Tecnología Avanzada-Unidad Legaria, Instituto Politécnico Nacional, C.P. 07738, Mexico,* [‡]*Departamento de Polímeros, Instituto de Investigaciones en Materiales, Universidad Nacional Autónoma de México, C.P. 04510, Mexico, and* [§]*Instituto de Ciencia y Tecnología de Materiales, Universidad de La Habana, Habana, Cuba*

Received August 4, 2009. Revised Manuscript Received September 28, 2009

In open framework Prussian blue analogues, all of the metal atoms linked at the N end of the CN groups are found at the surface of the cavities with an unsaturated coordination environment. These metal sites are available for a specific interaction with guest species. To shed light on the H_2 interaction with these metal sites, H_2 adsorption isotherms in $Ni_{3-x}Mn_x[Co(CN)_6]_2$, $Ni_{3-x}Co_x[Co(CN)_6]_2$, $Ni_{3-x}Cd_x[Co(CN)_6]_2$, and $Co_{3-x}Mn_x[Co(CN)_6]_2$ were recorded and evaluated. According to the obtained data for the adsorption heat values, the strongest H_2−metal interaction was found for Ni. The same evidence is obtained from the fitting of the isotherms using the osmotic model, where the value for the osmotic parameter (g) senses the strength for the guest−host interaction. The probable origin of that stronger interaction for the Ni atom is discussed. The information derived from these mixed series was complemented with an analogue study for $T_3[Co(CN)_6]_2$ and $T_3[Ir(CN)_6]_2$, with T = Mn, Co, Ni, Zn, Cu, and Cd. The strength for the guest−host interaction in these two simple series follows the order: Ni > Cu > Co ∼ Cd > Mn ∼ Zn. For the series $T_3[Co(CN)_6]_2$, H_2 adsorption isotherms up to 7600 Torr were recorded, confirming that the strongest H_2−metal interaction corresponds to Ni and Cu. The samples to be studied were characterized from energy-dispersed spectroscopy, X-ray diffraction, infrared, and CO_2 adsorption data.

1. Introduction

Hydrogen, because of its clean combustion (producing water as a byproduct), is being considered as potential replacement for fossil fuel derivatives, particularly for mobile technologies.[1] Fossil fuels are nonrenewable energy resources, and the emission of CO_2, as the main byproduct of their combustion, is responsible for global warming and the related climate changes. In addition, the oxidation of hydrogen liberates a large amount of energy, 142 kJ/g, 3 times the value obtained from gasoline (47.5 kJ/g). The use of hydrogen as an energy bearer involves three challenges: the production from the water splitting, for instance, because it is a secondary bearer and not a primary source, the availability of a safe and economically viable storage method, and its use through appropriate fuel cells. The concerning state of art suggests that a lot of basic research is required to support a hydrogen-based economy realization in the near future. With regard to the storage, all of the reported results remain short with respect to the technological requirements for practical applications. The established target [2015 U.S. Department of Energy (DOE) targets], in that sense, is 9 wt % for a reversible process and relatively short storage-release times.[2]

The difficulties for the H_2 storage are related to the weak H_2−H_2 intermolecular interactions (mainly of dispersive nature), which result in its low critical temperature (32.97 K). This is quite a low temperature to allow for H_2 handling in the liquid state for massive practical applications as combustible in mobile technologies, even when for years liquid H_2 has been used as fuel in test vehicles. Furthermore, the liquefaction process consumes about 40% of the energy to be generated. The storage in containers at high pressure also appears to be impractical, at least for mobile applications. For a pressure of 345 atm, a density of 22 g/L is obtained, relatively low compared to 71 g/L for the liquid state. From these facts, several routes are being studied to increase the storage density, among them, the physical adsorption in porous solids.[3−5] This is an attractive H_2 storage method because of its reversibility. However, to date, the reported gravimetric density of hydrogen adsorbed close to the atmospheric conditions remains well below the target of 9 wt %. Several families of porous materials have been evaluated in that sense, among them, carbon-based solids,[3] zeolites,[4] and metal−organic frameworks.[5−7] Recently, also porous coordination polymers, of Prussian blue (PB) type, have received

*To whom correspondence should be addressed. E-mail: ereguera@yahoo.com.

(1) Schlapbach, L.; Züttel, A. *Nature* **2001**, *414*, 353–358 and references therein.
(2) http://www.energy.gov/energysources/hydrogen.htm.
(3) Bhatia, S. K.; Myers, A. L. *Langmuir* **2006**, *22*, 1688–1700.
(4) Torres, F. J.; Civalleri, B.; Terentyev, A.; Ugliengo, P.; Pisani, C. *J. Phys. Chem. C* **2007**, *111*, 1871–878 and references therein.
(5) Rosi, N. L.; Eckert, J.; Eddaoudi, M.; Vodak, D. T.; Kim, J.; O'Keeffe, M.; Yaghi, O. M. *Science* **2003**, *300*, 1127–1129.
(6) Sun, D.; Ma, S.; Ke, Y.; Collins, D. J.; Zhou, H.-C. *J. Am. Chem. Soc.* **2006**, *128*, 3896–3897.
(7) Kaye, S. S.; Dailly, A.; Yaghi, O. M.; Long, J. R. *J. Am. Chem. Soc.* **2007**, *129*, 14176–14177 and references therein.

certain attention as the prototype of materials for H_2 storage studies.[8−16]

The ideal adsorption heat value to achieve the H_2 stabilization as adsorbed species close to atmospheric conditions has been estimated to be in the 20−30 kJ/mol range.[17] The reported H_2 adsorption heats related to van der Waals and electrostatic forces (H_2 polarization by a charge center and H_2 quadrupole moment interaction with the local electric field gradient) remain below that ideal range.[18−20] Fortunately, the hydrogen molecule behaves as a donor−acceptor ligand and forms coordination bonds with many transition metals, involving stabilization energy even higher than these ideal values.[21] From these features, the coordination of H_2 to metal centers appears as the paradigm for the hydrogen storage and has stimulated the H_2 adsorption study in porous solids with transition-metal ions with open coordination sites at the surface of cavities.[22−28] Among these solids, porous coordination polymers of PB type have also been considered.[8−16] In a previous study, we have reported evidence on the existence of a specific interaction between the hydrogen molecule and copper atoms found at the cavity surface of PB analogues.[15] The CN group has a certain ability to donate charge to the metal linked at its N end, increasing the electron density on the metal. In this contribution, the H_2 adsorption in anhydrous PB-type samples containing different metals at the surface of cavities is studied. Four mixed compositions were evaluated: $Ni_{3-x}Mn_x[Co(CN)_6]_2$, $Ni_{3-x}Co_x[Co(CN)_6]_2$, $Ni_{3-x}Cd_x[Co(CN)_6]_2$, and $Co_{3-x}Mn_x[Co(CN)_6]_2$. These mixed series were considered because Ni and Co are two metals with relatively high electron density at t_{2g} orbitals. Also, H_2 adsorption data for the simple series $T_3[Co(CN)_6]_2$ and $T_3[Ir(CN)_6]_2$ with T = Mn, Co, Ni, Zn, Cu, and Cd were recorded and evaluated. H_2 adsorption isotherms up to 10 atm were also recorded for the series $T_3[Co(CN)_6]_2$. For Ni^{2+}, evidence in favor of a relatively strong interaction with the hydrogen molecule was obtained. All of the samples were characterized from X-ray diffraction (XRD), infrared (IR), and energy-dispersed spectroscopy (EDS) data and CO_2 adsorption isotherms.

2. Experimental Section

The samples to be studied were prepared mixing 0.01 M aqueous solutions of potassium hexacyanometallate (Co and Ir) and sulfate of the involved metals. This is a simple and well-known synthetic route to obtain PB analogues.[8−16] The mixed series $Ni_{3-x}Mn_x[Co(CN)_6]_2$, $Ni_{3-x}Co_x[Co(CN)_6]_2$, $Ni_{3-x}Cd_x[Co(CN)_6]_2$, and $Co_{3-x}Mn_x[Co(CN)_6]_2$ were obtained from excess solutions of the involved metals at 1:1, 1:4, 1:6, and 1:8 atomic ratios. The use of the mixed metal solutions in excess relative to the complex anion guarantees that only a phase is formed. The formed precipitates were then separated by centrifugation, followed by successive washing with distilled water, and finally air-dried until they had a constant weight. The simple metal series, $T_3[Co(CN)_6]_2$ and $T_3[Ir(CN)_6]_2$, were prepared by the same procedure from solutions of the corresponding T metal sulfates. The reagents used were analytical-grade from Sigma-Aldrich. The nature of the obtained samples was established from XRD, EDS, and IR data. The hydration degree (number of water molecules per formula unit) and the thermal stability of the materials were estimated from thermogravimetric (TG) curves.

IR spectra were recorded in a FTIR spectrophotometer (Spectrum One from Perkin-Elmer) using the KBr pressed disk technique. EDS spectra were recorded using a spectrometer coupled to a scanning electron microscopy (SEM) microscope (from Jeol, Japan), also used to obtain SEM images for the materials under study. XRD powder patterns were collected using Cu Kα radiation, and their preliminary evaluation was carried out using Dicvol.[29] The framework stability and the cell contraction upon the crystal water removal and then cooling was evaluated from XRD powder patterns recorded at the X10B beamline of the Laboratório Nacional de Luz Síncrotron (LNLS) synchrotron radiation facility (Campinas, Brazil). TG curves were collected from 25 to 300 °C, under a N_2 flow (100 mL/min), using a TA Instruments thermo-balance (TGA 2950 model) operated in the high-resolution mode. The crystallite size was estimated from the obtained XRD data using the Scherrer equation[30] and SEM images.

The CO_2 and H_2 adsorption isotherms were recorded using an ASAP 2020 analyzer (from Micromeritics). Sample tubes of known weight were loaded with an appropriate amount of sample, ∼40 mg, and sealed using TranSeal. In this family of materials, the most reliable adsorption data, using an optimal measurement time, were obtained with a sample of about 50 mg. Previous to recording adsorption isotherms, the samples were degassed on the ASAP analyzer using a heating rate of 5 °C/min and then maintained at the dehydration temperature indicated by the TG curve until a stable outgas rate below 1 μm of Hg was obtained. This process usually requires 24 h of degassing. The degassed sample and sample tube were weighed and then transferred back to the analyzer (with the TranSeal to prevent exposure of the sample to air). After volume measurement with He, the degassing was continued for 24 h at 80 °C in the sample port. Measurements were performed using an ice−water bath for CO_2 and liquid N_2 and Ar baths for H_2. At the local atmospheric pressure (586 Torr), the boiling temperatures for N_2 and Ar are 75 and 85 K, respectively.

(8) Kaye, S. S.; Long, J. R. *J. Am. Chem. Soc.* **2005**, *127*, 6506–6507.
(9) Chapman, K. W.; Southon, P. D.; Weeks, C. L.; Kepert, C. J. *Chem. Commun.* **2005**, 3322–3324.
(10) Hartman, M. R.; Peterson, V. K.; Liu, Y.; Kaye, S. S.; Long, J. R. *Chem. Mater.* **2006**, *18*, 3221–3224.
(11) Culp, J. T.; Matranga, C.; Smith, M.; Bittner, E. W.; Bockrath, B. *J. Phys. Chem. B* **2006**, *110*, 8325–8328.
(12) Kaye, S. S.; Long, J. R. *Catal. Today* **2007**, *120*, 311–316.
(13) Natesakhawat, S.; Culp, J. T.; Matranga, C.; Bockrath, B. *J Phys. Chem. C* **2007**, *111*, 1055–1060.
(14) Reguera, L.; Krap, C. P.; Balmaseda, J.; Reguera, E. *J. Phys. Chem. C* **2008**, *112*, 10490–10501.
(15) Reguera, L.; Krap, C. P.; Balmaseda, J.; Reguera, E. *J. Phys. Chem. C* **2008**, *112*, 15893–15899.
(16) Ávila, M.; Reguera, L.; Rodríguez-Hernández, J.; Balmaseda, J.; Reguera, E. *J. Solid State Chem.* **2008**, *181*, 2899–2907.
(17) Zhao, Y.; Kim, Y. K.; Dillon, A. C.; Heben, M. J.; Zhang, S. B. *Phys. Rev. Lett.* **2005**, *94*, No. 155504-1-4.
(18) Turnes Palomino, G.; Llop Carayol, M. R.; Otero Areán, C *J. Mater Chem.* **2006**, *16*, 2884–2885.
(19) Reguera, L.; Balmaseda, J.; del Castillo, L. F.; Reguera, E. *J. Phys. Chem. C* **2008**, *112*, 5589–5597.
(20) Reguera, L.; Krap, C. P; Balmaseda, J.; Ávila, M.; Reguera, E. *J. Phys. Chem. C* **2008**, *112*, 17443–17449.
(21) Kubas, G. J. *Chem. Rev.* **2007**, *107*, 4152–4205.
(22) Chen, B.; Eddaoudi, M.; Reineke, T. M.; Kampf, J. W.; O'Keeffe, M.; Yaghi, O. M. *J. Am. Chem. Soc.* **2000**, *122*, 11559–11560.
(23) Forster, P. M.; Eckert, J.; Chang, J.-S.; Park, S.-E.; Férey, G.; Cheetham, A. K. *J. Am. Chem. Soc.* **2003**, *125*, 1309–1312.
(24) Schlichte, K.; Kratzke, T.; Kaskel, S. *Microporous Mesoporous Mater.* **2004**, *73*, 81–88.
(25) Rowsell, J. L. C.; Yaghi, O. M. *Angew. Chem., Int. Ed.* **2005**, *44*, 4670–4679.
(26) Chen, B.; Ockwig, N. W.; Millward, A. R.; Contreras, D. S.; Yaghi, O. M. *Angew. Chem., Int. Ed.* **2005**, *44*, 4745–4749.
(27) Dinca, M.; Dailly, A.; Liu, Y.; Brown, C. M.; Neumann, D. A.; Long, J. R. *J. Am. Chem. Soc.* **2006**, *128*, 16876–16883.
(28) Liu, Y.; Kabbour, H.; Brown, C. M.; Neumann, D. A.; Ahn, C. C. *Langmuir* **2008**, *24*, 4772–4777.
(29) Louer, D.; Vargas, R. *J. Appl. Crystallogr.* **1982**, *15*, 542–545.
(30) Guinier, A. *X-Ray Diffraction*; Dover Publications: Mineola, NY, 1994.

Table 1. Composition (x) and Unit Cell Parameters in (Å) for $T^A_{3-x}T^B_x[Co(CN)_6]_2\cdot yH_2O$, $T_3[Co(CN)_6]_2\cdot yH_2O$, and $T_3[Ir(CN)_6]_2\cdot yH_2O$[a]

T^A	$T^B\rightarrow$	Mn	Co	Ni	Cd	T_3Co_2	T_3Ir_2
Mn		10.421 (1)	x = 1.2, 10.350(2); x = 1.8, 10.312 (1)	x = 1.3, 10.318 (1); x = 1.8, 10.253 (2);	b	10.267(3)	10.192(1)
Co		x = 1.2, 10.350(2); x = 1.8, 10.312 (1)	10.220(1)	x = 1.7, 10.184 (1)	b	10.2805(3)	10.228(1)
Ni		x = 1.3, 10.318 (1); x = 1.8, 10.253 (2);	x = 1.7, 10.184 (1)	10.162 (1)	x = 1.5, 10.370(1)	10.262(1)	10.216(1)
Cd		b	b	x = 1.5, 10.370 (1)	10.591(1)	10.216(1)	10.183(1)

[a] $T_3Co_2 \equiv T_3[Co(CN)_6]_2\cdot yH_2O$, and $T_3Ir_2 \equiv T_3[Ir(CN)_6]_2\cdot yH_2O$. [b] Solid solutions not studied. This family of solids crystallizes with a cubic unit cell (*Pm3m* space group).

The obtained H_2 adsorption data were fitted using the Osmotic isotherm[31]

$$P_{eq} = P_{0.5}\left(\frac{n_{ad}}{n_p - n_{ad}}\right)^g \quad (1)$$

where n_{ad} is the amount adsorbed at the equilibrium pressure P_{eq}, n_p is the the limiting amount filling the micropores, $P_{0.5}$ is the equilibrium pressure at $n_p/2$, and g is the osmotic coefficient related to ideality of the solution. Previous studies on the hydrogen adsorption in porous cyanometallates indicate that the value of g can be used as a sensor for the strength of the guest−host interaction.[14−16,19,20]

The enthalpy of adsorption (ΔH_{ads}) was obtained by the isosteric method from isotherms recorded at N_2 and Ar baths and then using a variant of the Clausius−Clapeyron equation to calculate the ΔH_{ads} value according to[32]

$$\ln\left(\frac{P_1}{P_2}\right) = \frac{\Delta H_{ads}}{R}\frac{T_2 - T_1}{T_1 T_2} \quad (2)$$

where T_1 and T_2 are temperatures of the used baths, in this case 75 K (N_2) and 85 K (Ar).

To shed light on the strength of the guest−host interaction and its dependence upon the metal found at the cavity surface, for the series $T_3[Co(CN)_6]_2$, H_2 adsorption isotherms up to 10 atm were also recorded, in this case using an ASAP 2050 analyzer.

3. Results and Discussion

3.1. Characterization of the Samples To Be Studied. The formula units for $T_3[Co(CN)_6]_2\cdot yH_2O$ and $T_3[Ir(CN)_6]_2\cdot yH_2O$ with T = Mn, Co, Ni, Cu, Zn, and Cd are supported by the metal atomic ratios, close to 3:2, obtained from the EDS data. For the mixed series, $Ni_{3-x}Mn_x[Co(CN)_6]_2\cdot yH_2O$, $Ni_{3-x}Co_x[Co(CN)_6]_2\cdot yH_2O$, $Ni_{3-x}Cd_x[Co(CN)_6]_2\cdot yH_2O$, and $Co_{3-x}Mn_x[Co(CN)_6]_2\cdot yH_2O$, the Ni/Mn, Ni/Co, Ni/Cd, and Co/Mn atomic ratios found for the precipitated powders were quite different from those in the initial solutions (Table 1). This suggests that the involved metals have different affinities for the N end of the CN group. The metal binding to the CN group at the N end takes place through the ligand 5σ orbital, which donates charge to the metal. Then, the mentioned affinity is related to the metal ability to subtract charge from the ligand. As a sensor for that ability, the metal polarizing power can be taken, which for the considered metals follows the order Ni > Co > Mn > Cd.[33] This coincides with the order of affinity derived from the atomic ratio of the metals obtained from the recorded EDS spectra (Table 1).

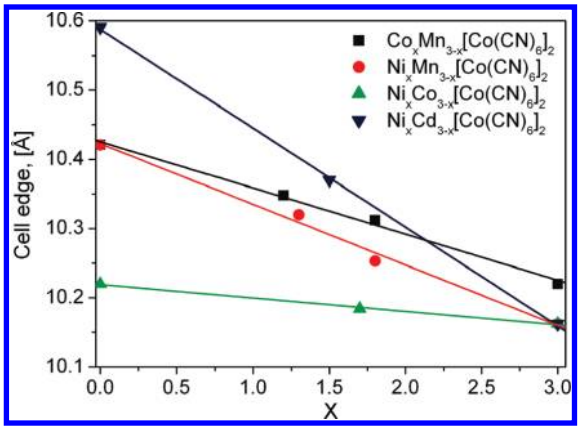

Figure 1. Correlations between the unit cell edge, a (the T−N≡C−M−C≡N−T chain length), and the amount of the second metal found at the cavity surface. These linear relationships are typical of the formation of true solid solutions. Error bars for x and cell edge values remain below the symbol size.

PB analogues crystallize with a cubic unit cell related to an octahedral coordination also for the metal linked at the N end of the CN ligands.[34] The metal linked at the C end is always found with an octahedral coordination. According to Mössbauer spectra of PB analogues containing Fe^{2+} linked at the N end, the structure of this family of compounds contains two well-defined structural sites for the outer metal.[35−37] This corresponds to a primitive space group (*Pm3m*), which has also been observed in PB samples recrystallized in concentrate HCl.[38] The (T^AT^B)−N≡C−Co−C≡N−(T^AT^B) chain length, which coincides with the cell edge (a) for PB analogues, and the atomic ratio of T^A and T^B metals in these mixed series were found to be linearly correlated (Figure 1). Such a correlation is in accordance with the empirical rule known as Vegard's law,[39] which relates the unit cell constant with the elemental composition of a solid solution or alloy. The linear relations shown in Figure 1 indicate that the obtained mixed series correspond to true solid solutions. In the mixed series, the involved outer metals ($Ni_{3-x}Co_x$, $Ni_{3-x}Cd_x$, $Co_{3-x}Mn_x$, and $Co_{3-x}Mn_x$) are randomly distributed on the cavity surface of the material structure. Figure 2 illustrates the available free spaces for this family of materials. Relatively large cavities of ca. 8.5 Å in

(31) Bering, B. P.; Serpinskii, V. V. *Izv. Akad. Nauk SSSR Ser. Khim.* **1974**, *11*, 2427–2437.
(32) Rouquerol, F.; Rouquerol, J.; Sing, K. *Adsorption by Powders and Solids: Principles, Methodology and Applications*; Academic Press: London, U.K., 1999.
(33) Zhang, Y. *Inorg. Chem.* **1982**, *21*, 3886–3889.
(34) Ludi, A.; Gudel, H. U. *Struct. Bonding* **1973**, *14*, 1–21.
(35) Reguera, E.; Yee-Madeira, H.; Fernandez-Bertran, J.; Nuñez, L. *Transition Met. Chem.* **1999**, *24*, 163–167.
(36) Krap, C. P.; Zamora, B.; Reguera, L.; Reguera, E. *Microporous Mesoporous Mater.* **2009**, *120*, 414–420.
(37) Reguera, E.; Yee-Madeira, H.; Demeshko, S.; Eckold, G.; Jiménez-Gallegos, J. *Z. Phys. Chem.* **2009**, *223*, 701–711.
(38) Buser, H. J.; Schwarzenbach, D.; Petter, W.; Ludi, A. *Inorg. Chem.* **1977**, *16*, 2704–2710.
(39) Denton, A. R.; Ashcroft, N. W. *Phys. Rev. A: At., Mol., Opt. Phys.* **1991**, *43*, 3116.

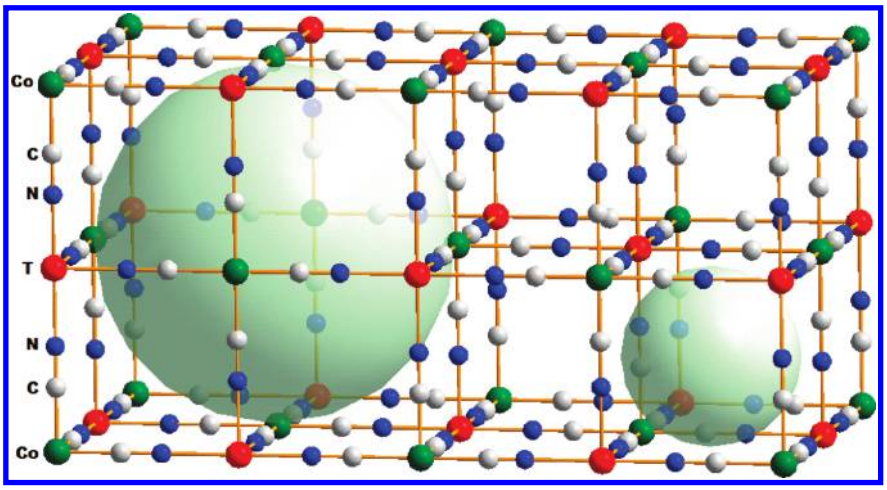

Figure 2. Framework of porous PB analogues. Relatively large cavities (larger sphere) of ca. 8.5 Å in diameter generated by a vacancy for the building block remain communicated by the interstitial spaces (smaller sphere) of about 4.5 Å.

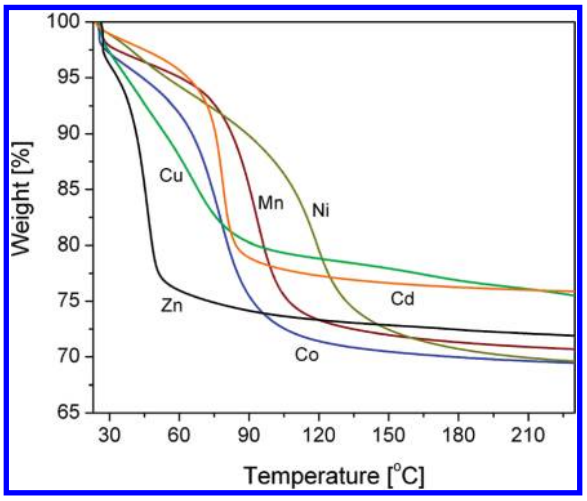

Figure 3. TG curves for the series $T_3[Co(CN)_6]_2 \cdot yH_2O$. An analogue behavior upon heating was observed for the iridium series, $T_3[Ir(CN)_6]_2 \cdot yH_2O$. For Ni, the strongest H_2O−metal interaction is observed (the highest dehydration temperature) related to a relatively high polarizing power for the Ni atom.

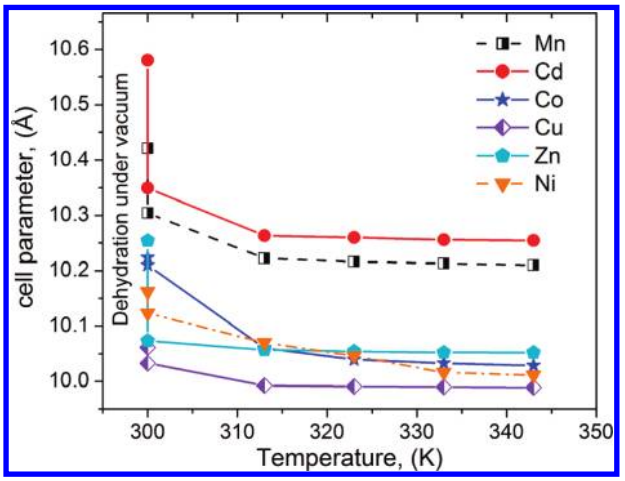

Figure 4. Cell contraction on the water removal for the series $T_3[Co(CN)_6]_2$. Under only vacuum (10^{-6} Torr at 300 K), without heating, a large fraction of the crystal water is removed. The error bar for the cell parameter value remains below the symbol size.

diameter remain communicated by the interstitial spaces of about 4.5 Å (smaller sphere in Figure 2). According to the formula unit and structure of the materials, in some framework regions, contiguous (fused) cavities of 8.5 Å can also be found. PB analogues are usually obtained as microcrystalline powders formed from small cubic crystals of about 100 nm in size (see Table 1 and the Supporting Information).

Porous PB analogues are highly hydrated solids with both coordinated and weakly bonded water molecules. The coordination sphere for the metal found at the cavity surface is completed with water molecules, and these last ones contribute to the stabilization of additional water molecules within the cavity through hydrogen-bonding interactions. Both weakly bonded and coordinated water molecules evolve upon heating, usually below 120 °C, to obtain an anhydrous porous solid that remains stable up to 250 °C (see Figure 3). In the presence of two different metals at the cavity surface, the material dehydrates at an intermediate temperature between those observed for the corresponding simple metal compositions.[40,41] Figure 4 shows the unit cell parameter variation for the series $T_3[Co(CN)_6]_2 \cdot yH_2O$ on the crystal water removal. The cell contraction on the dehydration is equivalent to a reduction for the M−C−N−T interatomic distances. In the anhydrous phase, the T metal only interacts with the framework ligands, increasing the charge subtraction from the CN groups. This induces a greater π-back donation from the inner metal (M). The charge removed by this mechanism is mainly located on the N end and partially donated to the metal located at the cavity surface. This is detected as an increase for the superexchange interaction among M and T metals and as an increase for the temperature of magnetic order (Tc) when the samples are dehydrated.[42] Analogue evidence is obtained when Mössbauer spectra of hydrated and anhydrous ferricyanide samples are compared.[40,42,43] The material

(40) Balmaseda, J.; Reguera, E.; Rodríguez-Hernández, J.; Reguera, L.; Autie, M. *Microporous Mesoporous Mater*. **2006**, *96*, 222–236.

(41) Roque, J.; Reguera, E.; Balmaseda, J.; Rodríguez-Hernández, J.; Reguera, L.; del Castillo, L. F. *Microporous Mesoporous Mater*. **2007**, *103*, 57–71.

(42) Martínez-García, R.; Knobel, M.; Reguera, E. *J. Phys.: Condens. Matter* **2006**, *18*, 11243–11254.

(43) Martínez-García, R.; Knobel, M.; Reguera, E. *J. Phys. Chem. B* **2006**, *110*, 7296–7303.

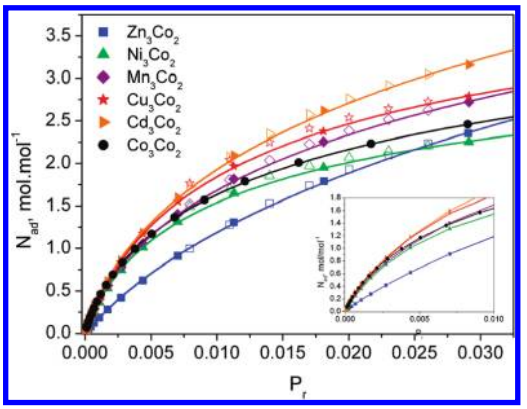

Figure 5. CO_2 adsorption isotherms for the series $T_3[Co(CN)_6]_2$. (Inset) Region of low coverage (low pressures) for the same isotherms.

dehydration leads to an increase for the electron density on the metal located at the cavity surface, reducing the surface polarizing power for the guest species with the cavity. For Zn, the material can be dehydrated under vacuum at room temperature. In the anhydrous cubic phase, the Zn atom adopts a pseudo-tetrahedral coordination.[41] For copper, the dehydration temperature is about 60 °C.

Because H_2 adsorption experiments were carried out under cryogenic conditions, the evaluation of the material behavior at cryogenic temperatures was studied. According to XRD data recorded at 77 and 12 K, no structural changes upon cooling were observed. Relative to room-temperature anhydrous samples, the cell volume reduction upon cooling remains below 1%. This agrees with the reported zero or negative thermal expansion for PB analogues.[44]

The porous framework for the anhydrous samples was also characterized from CO_2 adsorption data. Figure 5 shows the recorded CO_2 adsorption isotherms for the series $T_3[Co(CN)_6]_2$. Analogues isotherms were obtained for the iridium series, $T_3[Ir(CN)_6]_2$, and also for the mixed compositions (see the Supporting Information). Their porous framework is accessible to the CO_2 molecule. According to the slope of these isotherms for the region of low relative pressures (low coverage), the strength of the guest−host interaction for CO_2 is practically independent of the metal found at the cavity surface. Such behavior was attributed to the relatively large size of that molecule, with ca. 2.40 Å length, and also to its rotational state (at 273 K, the CO_2 molecule is rotating). For a linear molecule, such as CO_2, the dispersive and polarization interactions reach their maximum strength when the molecule is accommodated parallel to the cavity surface. The observed deviation for T = Zn was attributed to the poor accessibility of the guest molecule to the Zn atom environment.[41] In anhydrous zinc hexacyanometallates (III), the Zn atom is found with a pseudo-tetrahedral coordination. This leads to a relatively large CO_2−surface distance and a weak adsorption potential for this molecule.

3.2. Properties of H_2 and Nature of the Adsorption Interactions. The adsorption forces are determined by both the adsorbate and adsorbent properties. Hydrogen is a molecule with a permanent quadrupole moment (Q). From this fact, it is able to interact with an electric field gradient ($\nabla \boldsymbol{E}$).

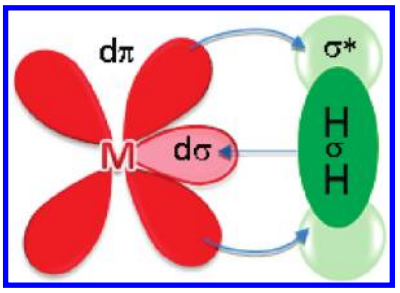

Figure 6. Side-on H_2 coordination to a transition-metal ion (M). The hydrogen molecule behaves as a donor−acceptor ligand.

The interaction energy ($E = -(1/3)Q\nabla \boldsymbol{E}$) depends upon r^{-3} (r is the distance between the guest species and the charge center responsible for $\nabla \boldsymbol{E}$). Hydrogen has a positive Q value (0.4926 in atomic units, ea_o^2)[45] and, in consequence, is oriented with the molecular axis (the imaginary line that joins the two H atoms) perpendicular to $\nabla \boldsymbol{E}$. The positive sign for Q also explains that, in highly condensed states, H_2 molecules are stacked in a crossed configuration, where the molecular axis of a given molecule remains perpendicular to that of the neighboring ones.

In the presence of a positive charge center, the H_2 electron cloud can be polarized. The contribution in energy (E) of this attractive interaction to the adsorption energy depends upon both the molecule polarizability (α) and the local electric field ($\boldsymbol{E}$), $E = (1/2)\alpha/\boldsymbol{E}^2$. This interaction depends upon r^{-4}. Such dependence upon r suggests that it becomes relevant only for relatively short adsorbent−adsorbate distances. For H_2, that interaction is most favorable when the molecules are oriented with the molecular axis parallel to the adsorbent surface. For H_2, the value of α is 0.8023, in 10^{-24} cm^3 units.[46] Hydrogen is the smallest molecule in nature, with only two electrons, which are involved in a σ bond. This explains the relatively small value of α for H_2, the smallest one for common molecules.[46]

The dispersive forces (also known as van der Waals type interactions), related to the resonant fluctuations of the adsorbent and adsorbate electron clouds also contribute to the adsorption processes. Such fluctuations for the charge distributions are responsible for induced dipole and quadrupole moments and lead to attractive adsorbent−adsorbate interactions. These are short distance forces, which depend upon r^{-6}. The strength of the dispersive interactions also depends upon the amount of involved electrons. When the overlapping between the electron clouds is quite pronounced, the repulsive contribution because of the exchange interaction, which depends upon r^{-12}, dominates.[32]

In addition to the above-mentioned interactions, of physical nature, H_2 can also form a coordination bond to transition metals without the molecule dissociation. As already-mentioned, the H_2 binds side on to the metal center through σ donation to a vacant metal d orbital. This interaction is stabilized when a fraction of the metal electrons populates the H_2 σ* orbital by means of a back-bonding interaction, which is favorable for metals with high electron density on their t_{2g} orbitals (see Figure 6). For hydrogen, all of the mentioned adsorption forces lead to a side-on

(44) Chapman, K. W.; Chupas, P. J.; Kepert, C. J. *J. Am. Chem. Soc.* **2006**, *128*, 7009–7014.

(45) Lochan, R. C.; Head-Gordon, M. *Phys. Chem. Chem. Phys.* **2006**, *8*, 1357–1370.

(46) *CRC Handbook of Chemistry and Physics*, 84th ed.; Lide, D. R., Ed.; CRC Press: Boca Raton, FL, 2003−2004.

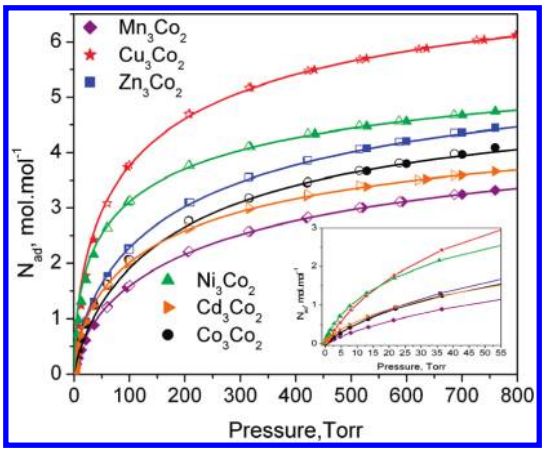

Figure 7. H_2 adsorption isotherms for the series $T_3[Co(CN)_6]_2$, with T = Mn, Co, Ni, Cu, Zn (cubic phase), and Cd, including the desorption data (open symbols). (Inset) Region of low pressures for these isotherms.

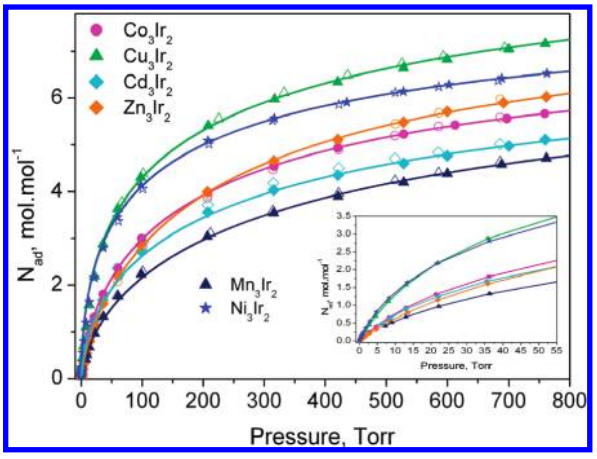

Figure 8. H_2 adsorption isotherms for the series $T_3[Ir(CN)_6]_2$, with T = Mn, Co, Ni, Cu, Zn (cubic phase), and Cd, including the desorption data (open symbols). (Inset) Region of low pressures for the same isotherms.

interaction with the adsorption site and between neighboring adsorbed molecules.

3.3. Hydrogen Adsorption Isotherms. Hydrogen storage in the $T_3[Co(CN)_6]_2$ series has already been reported[8,9] but with quite different results among these two papers regarding the adsorbed amount dependence upon the metal found at the cavity surface. From this fact, the H_2 storage in that series of PB analogues was reconsidered, also including the series corresponding to iridium as an inner metal, $T_3[Ir(CN)_6]_2$, not previously studied. Figures 7 and 8 show the recorded H_2 adsorption isotherms for these two simple metal series. According to the isotherm slope for the region of low pressures, the guest−host strength interaction follows the order Ni > Cu > Co ~ Cd ~ Zn > Mn. For Ni and Cu, that order agrees with the reported one from the adsorption heats measured for the hexacyanocobaltate (III) series.[8] When these isotherms are fitted using the osmotic model (eq 1), the order for maximum adsorption, extrapolated at $P \rightarrow \infty$ (see Table 2), results in Cu > Zn > Ni > Co > Cd > Mn. This order shows some differences regarding the obtained one for the strength of the guest−host interaction from the isotherm slope at low pressure. For instance, for Cu and Ni, with similar isotherm slopes, the maximum amounts adsorbed are quite different. Such behavior could be related to the vacancy distribution within the solid structure. To a totally random vacancy distribution, the solid has the minimum available free volume and at the inverse for a material of ordered vacancies. This last case corresponds to Cu, where the XRD powder pattern belongs to the *Pm*3*m* space group.[43] The observed variation for the maximum amount adsorbed could be attributed to a different degree of disorder for the vacancies within the structure. The vacancy distribution also determines the amount and nature of available metal sites to interact with the hydrogen molecule. To a random distribution, five types of sites correspond, with the following coordination environments for the outer metal: $T(NC)_1$, $T(NC)_2$, $T(NC)_3$, $T(NC)_4$, and $T(NC)_5$. Their relative populations in the structure are 10, 24, 32, 24, and 10%, respectively.[35] A structure of ordered vacancies (*Pm*3*m*) contains only two types of sites, TN_3 and TN_5, with approximately the same relative population.[37]

Figures 9−12 show the recorded H_2 adsorption isotherms for the mixed series. These isotherms are conclusive regarding the role of the metal found at the cavity surface for the H_2 storage in PB analogues. For the $Ni_{3-x}Mn_x[Co(CN)_6]_2$ series, for instance, the substitution of Ni atoms by Mn always leads to a weakening for the H_2−metal interaction and also the maximum amount of H_2 adsorbed. The same behavior is observed for the $Ni_{3-x}Cd_x[Co(CN)_6]_2$ and $Ni_{3-x}Co_x[Co(CN)_6]_2$ series. The effect is less pronounced for the $Co_{3-x}Mn_x[Co(CN)_6]_2$ series because, according to the results for the simple series, these two metals have similar ability to interact with the hydrogen molecule.

For hydrogen, the role of the metal on the adsorption potential is quite different from that observed for carbon dioxide. Hydrogen is a relatively small molecule, of approximately 0.76 Å of interatomic distance,[21] similar to the ionic radius for the involved T metals.[47] This favors a highly localized interaction for H_2 with the metal, a relatively short H_2−metal distance, and a greater contribution of the electrostatic and coordination interactions to the adsorption potential.

All of the recorded H_2 adsorption isotherms were fitted using the osmotic model (eq 1). Table 2 summarizes the obtained values for model parameters. The values calculated for the osmotic parameter (*g*) parallels the above-discussed regularity from the isotherm slope in the low coverage region. The *g* value is sensing the guest−host interaction strength.

The adsorption heat (ΔH_{ad}) values for the H_2 adsorption, calculated by the isosteric method from isotherms recorded at 75 and 85 K using eq 2, are collected in Table 2. Figures 13 and 14 show the dependence of ΔH_{ad} on the amount adsorbed for T = Cu, Ni, Co, and Mn in the two simple series, $T_3[Co(CN)_6]_2$ and $T_3[Co(CN)_6]_2$, and for the low coverage region. The ΔH_{ad} values reported in Table 2 corresponds to the maximum value obtained from the ΔH_{ad} versus n_{ads} curves (Figures 13 and 14). The isotherms recorded using N_2 and Ar baths are available from the Supporting Information. The obtained ΔH_{ad} values are in the 5−8 kJ/mol range, similar to those already reported for the $T_3[Co(CN)_6]_2$ series.[8]

Among the values of ΔH_{ad} and *g* (Table 2), a positive correlation is appreciated. To an increase for ΔH_{ad}, a greater

(47) Shannon, R. D. *Acta Crystallogr., Sect. A: Found. Crystallogr.* **1976**, *32*, 751–767.

Table 2. Results Derived from the H_2 Adsorption Isotherms Fitting According to the Osmotic Model[a]

compound	temperature (K)	n_p (mol/mol)	H_2 molecules per cavity	g	ΔH_{ads} (kJ/mol)	H_2 (wt %)
$Mn_3[Co(CN)_6]_2$	75	5.07 ± 0.11	5.07	1.43 ± 0.02	5.7	1.71
	85	4.1 ± 0.1	4.1	1.12 ± 0.03		1.38
$Co_3[Co(CN)_6]_2$	75	5.38 ± 0.09	5.38	1.21 ± 0.02	6.2	1.77
	85	5.21 ± 0.07	5.21	1.18 ± 0.02		1.72
$Ni_3[Co(CN)_6]_2$	75	6.47 ± 0.01	6.47	1.88 ± 0.07	7.3	2.14
	85	6.31 ± 0.23	6.31	1.38 ± 0.07		2.09
$Cu_3[Co(CN)_6]_2$	75	8.1 ± 0.2	8.1	1.65 ± 0.06	6.9	2.61
	85	7.2 ± 0.2	7.2	1.30 ± 0.04		2.32
$Zn_3[Co(CN)_6]_2$	75	6.30 ± 0.24	6.30	1.43 ± 0.02		2.03
$Cd_3[Co(CN)_6]_2$	75	5.16 ± 0.11	5.16	1.52 ± 0.03		1.34
$Mn_3[Ir(CN)_6]_2$	75	7.79 ± 0.65	7.79	1.47 ± 0.03	5.9	1.81
	85	5.71 ± 0.10	5.71	1.10 ± 0.01		1.32
$Co_3[Ir(CN)_6]_2$	75	8.01 ± 0.08	8.01	1.44 ± 0.04	6.5	1.83
	85	7.80 ± 0.06	7.80	1.18 ± 0.01		1.78
$Ni_3[Ir(CN)_6]_2$	75	8.91 ± 0.08	8.91	1.76 ± 0.04	7.20	2.04
	85	8.61 ± 0.06	8.61	1.22 ± 0.03		1.98
$Cu_3[Ir(CN)_6]_2$	75	10.6 ± 0.5	10.6	1.8 ± 0.1	7.18	2.39
	85	9.3 ± 0.3	9.3	1.50 ± 0.06		2.10
$Zn_3[Ir(CN)_6]_2$	75	8.63 ± 0.24	8.63	1.31 ± 0.05		1.94
$Cd_3[Ir(CN)_6]_2$	75	7.92 ± 0.17	7.92	1.58 ± 0.02		1.52
$Co_{1.6}Mn_{1.4}[Co(CN)_6]_2$	75	5.3 ± 0.22	5.3	1.40 ± 0.08	5.9	1.76
	85	5.1 ± 0.22	5.10	1.23 ± 0.01		1.70
$Co_{1.2}Mn_{1.8}[Co(CN)_6]_2$	75	5.19 ± 0.20	5.19	1.49 ± 0.02	5.7	1.73
	85	4.93 ± 0.28	4.93	1.23 ± 0.04		1.64
$Ni_{1.8}Mn_{1.2}[Co(CN)_6]_2$	75	6.30 ± 0.24	6.30	1.60 ± 0.01	6.45	2.10
	85	5.72 ± 0.22	5.72	1.34 ± 0.04		1.91
$Ni_{1.3}Mn_{1.7}[Co(CN)_6]_2$	75	5.30 ± 0.16	5.30	1.69 ± 0.07	7.04	1.77
	85	4.90 ± 0.12	4.90	1.40 ± 0.03		1.64
$Ni_{1.5}Cd_{1.5}[Co(CN)_6]_2$	75	7.43 ± 0.32	7.43	1.54 ± 0.09		2.16
$Ni_{1.5}Co_{1.5}[Co(CN)_6]_2$	75	7.28 ± 0.11	7.28	1.73 ± 0.03		2.41

[a] n_p, limit capacity of micropores; g, osmotic coefficient; H_2/cavity, estimated limit amount of H_2 molecules per cavity; and wt %, maximum estimated adsorption in weight percent.

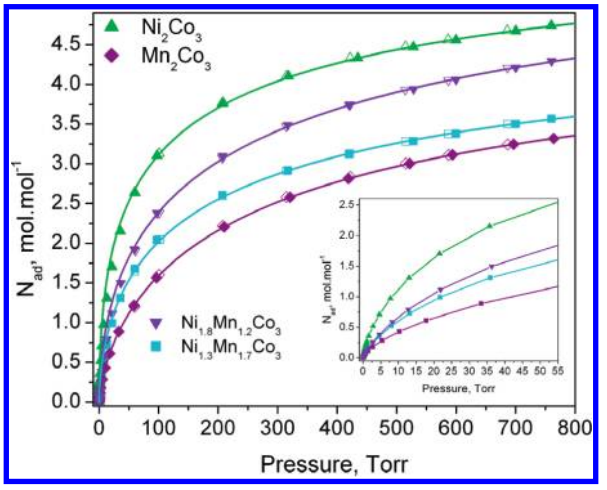

Figure 9. H_2 adsorption isotherms for the mixed series $Ni_{3-x}Mn_x[Co(CN)_6]_2$, including the desorption data (open symbols). (Inset) Region of low pressures for the same isotherms.

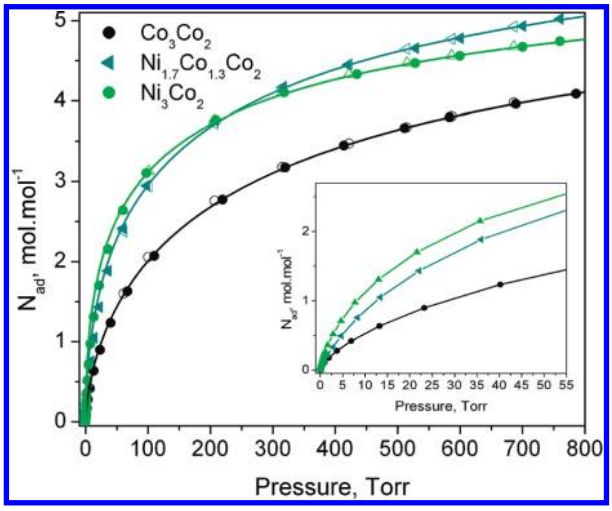

Figure 10. H_2 adsorption isotherms for the mixed series $Co_{3-x}Ni_x[Co(CN)_6]_2$, including the desorption data (open symbols). (Inset) Region of low pressures for the same isotherms.

value of g always corresponds. However, unlike ΔH_{ad}, the osmotic coefficient is an empirical parameter without a direct physical meaning. Nevertheless, such a correlation has practical usefulness because the g value can be used as a sensor for the strength of the guest−host interaction in comparative studies of materials for hydrogen storage. To estimate the value of g, only a single isotherm is required.

3.4. High-Pressure H_2 Adsorption Isotherms. In adsorption studies, two concepts are usually involved, excess and absolute adsorption. The recorded isotherms usually correspond to the excess adsorption, which is the amount of adsorbate molecules that are retained (adsorbed) by the interaction with the surface. The absolute adsorption senses the excess adsorption plus the amount of adsorbate molecules that occupies the available free volume within the porous framework in the absence of adsorption forces. Figure 15 shows the H_2 adsorption isotherms (excess adsorption) up to 7600 Torr for the series $T_3[Co(CN)_6]_2$. For Ni and Cu, the excess adsorption reaches a maximum and then decreases. The same behavior is observed for Co and Cd but less pronounced. The maximum occurs at the pressure where the gas densities at the sample pore and the bulk gas are increasing at the same rate, so that a pressure increase has no effect on the amount adsorbed. Above that point, the gas density in the sample pores saturates, while the bulk gas density keeps increasing, resulting in the observed

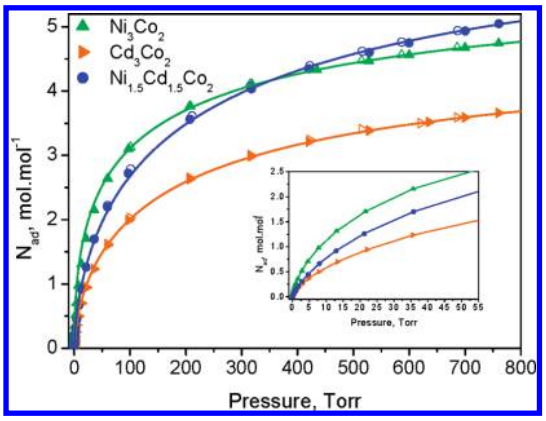

Figure 11. H_2 adsorption isotherms for the mixed series $Ni_{3-x}Cd_x$-$[Co(CN)_6]_2$, including the desorption data (open symbols). (Inset) Region of low pressures for the same isotherms.

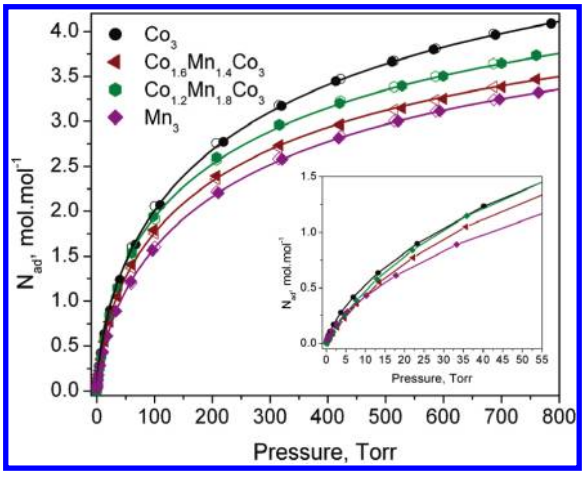

Figure 12. H_2 adsorption isotherms for the mixed series $Co_{3-x}Mn_x$-$[Co(CN)_6]_2$, including the desorption data (open symbols). (Inset) Region of low pressures for the same isotherms.

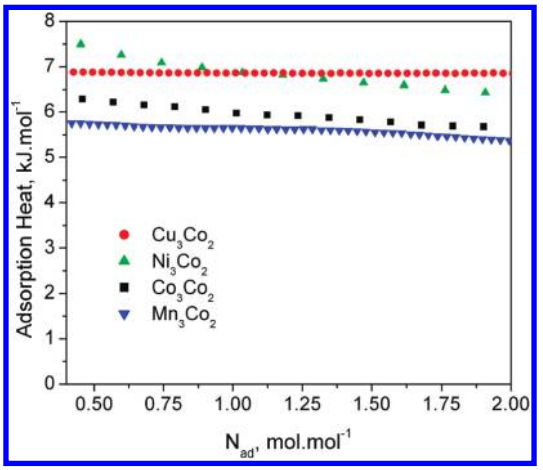

Figure 13. Curves of hydrogen adsorption heats for $T_3[Co(CN)_6]_2$.

negative gain for the excess amount adsorbed. A strong guest−host interaction leads to a rapid saturation of the adsorption sites, and the maximum for the excess adsorption isotherm is observed at a relatively low pressure. According to this criterion, the order for the strength of the guest−host interaction for H_2 in the PB analogues under study is Ni > Cu > Co ∼ Cd > Mn ∼ Zn. This order is similar to that derived from the isotherm slope at low pressures.

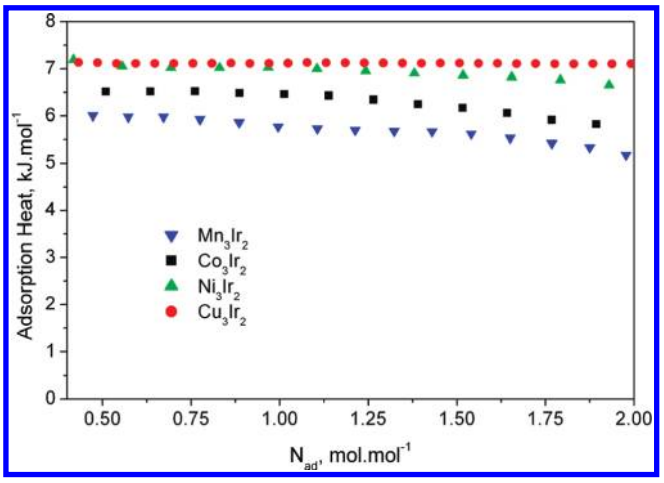

Figure 14. Curves of hydrogen adsorption heats for $T_3[Ir(CN)_6]_2$.

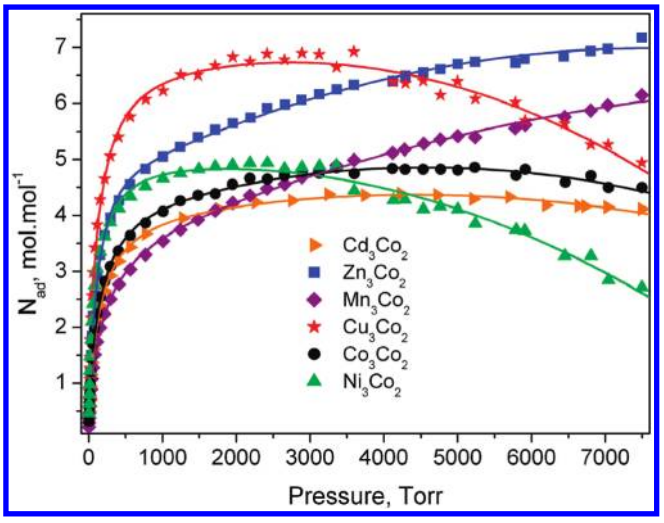

Figure 15. High-pressure H_2 adsorption isotherms (excess adsorption) at 75 K for $T_3[Co(CN)_6]_2$.

Within the metals where the excess adsorption has a definite maximum, Cu, Ni, Co, and Cd, the highest adsorption capacity was observed for Cu, above 40% of the value obtained for the remaining metals. Such behavior was attributed to the already discussed non-random vacancy distribution for the structure of copper PB analogues.

The unique behavior observed for Cd (Figure 15), a big metal with a low polarizing power, where the excess adsorption shows saturation, a feature not shown by Mn for instance, can be ascribed to a significant contribution of dispersive-type interactions to the adsorption forces. The cadmium (2+) atom has a large amount of electrons (46), and this favors the induction of instantaneous dipole and quadrupole moments by resonant fluctuations of the electron cloud during its interaction with the hydrogen molecule.

3.5. On the Nature of the H_2−Metal Interaction. The value for ΔH_{ad} from van der Waals type interactions, as those present during the H_2 adsorption in carbon-based materials, remains below 5 kJ/mol.[3] The adsorption heat values obtained for PB analogues, even for Mn, are above that value. This suggests that, in this family of compounds, other adsorption forces are contributing to the H_2 storage. Their cavity surface and, particularly, the metal centers behave as positive-charge centers capable of polarizing the electron

cloud of guest species within the cavity. This explains that porous PB analogues are always obtained as hydrated materials. From these features, for this family of porous solids, a certain charge polarization interaction must be contributing to the adsorption potential for the hydrogen molecule. Such charge centers must also be responsible for the existence of an electric field gradient within the cavity, also contributing to the H_2 adsorption.

The presence of at least a week interaction of H_2 coordination to the metal centers cannot be discarded, particularly for Ni. Ni^{2+} has a $3d^8$ electronic configuration, and the interaction with the CN ligand at the N end is particularly strong. As a sensor of that interaction, the ν(CN) vibration frequency can be used, which for Ni is 2180 and 2179 cm^{-1} for M = Co and Ir, respectively. These frequency values are within the highest ones for PB analogues.[48] From these facts, the effective electronic configuration for the Ni atom is $3d^{(8+\delta)}$. The electron density on the Ni atom ($8 + \delta$) is additionally increased when the material is dehydrated. As already discussed, a high electron density on the t_{2g} orbitals is a favorable condition for the H_2 coordination to a metal center because such electron availability allows the metal charge donation to the σ^* orbital of the hydrogen molecule (Figure 6). However, we believe that the relatively strong H_2−Ni interaction observed in PB analogues is related to electrostatic-type forces. The Ni atom at the cavity surface preserves a relatively high polarizing power, as suggested by the temperature value required to remove its coordinated water molecules, the highest one within PB analogues (Figure 3). Analogue evidence is obtained from the variation of the cell edge on the sample heating under high vacuum (Figure 4). A quite different nature has the H_2 interaction with the copper atom in PB analogues because the effective polarizing power for the copper atom at the cavity surface is the lowest one within this family of compounds. In PB analogues, the electronic configuration for the copper atom is close to $3d^{10}$.[48] The H_2 adsorption in copper hexacyanometallates has been discussed considering that a certain interaction of coordination type is present.[15]

The discrimination between the electron cloud polarization and coordination interactions for the case of Ni, using IR spectroscopy, for instance,[49] has a limited scope, because for the two interactions, the same effect on the ν(H−H) vibration is expected. The polarization of the H_2 electron cloud behaves as "coordination" to the charge center.

The above-discussed results on the amount of H_2 adsorbed in PB analogues remain below the established requirement (target) for hydrogen storage applications in mobile technologies.[2] However, these results serve to shed light on the scope of the H_2−metal interaction for metal located at the surface of the cavities. The involved H_2 adsorption energy is well above the values corresponding to dispersive-type interactions but below the technological requirements (20−30 kJ/mol).[3] An option to increase the ΔH value is the H_2 interaction, with bare transition metals within the cavities of porous solids. At least for Cu^+ within the cavities of zeolites, the results reported are highly promising, with ΔH values in the 39−73 kJ/mol range.[50,51]

4. Conclusions

The hydrogen adsorption was studied in two families of simple PB analogues, $T_3[Co(CN)_6]_2$ and $T_3[Ir(CN)_6]_2$, and in four mixed compositions. The adsorption potential for the hydrogen molecule in PB analogues follows the order Ni > Cu > Zn ∼ Co ∼ Cd > Mn. The adsorption potential sensed by the hydrogen molecule is determined by the metal properties (polarization power and local electric field gradient) and not the cavity surface, as an average. This is possible because the size of the hydrogen molecule is similar to the metal ionic radius. Except for Cu, the obtained results suggest that, for the remaining metals, the H_2 adsorption potential is dominated by electrostatic and van der Waals (dispersive) type forces. Within PB analogues, the Ni atom located at the cavity surface preserves a relatively high polarizing power, which determines its strong electrostatic interaction with the hydrogen molecule, a mechanism that cannot be attributed to copper because of its high electron density, close to $3d^{10}$, and low polarizing power. For the maximum H_2 adsorbed molecules, a relatively large variation on the metal found on the cavity surface was observed, which was ascribed to the distribution mode for the building block vacancies within the material structure. The amount of H_2 molecules that can be accumulated in excess within the porous framework of PB analogues and the related adsorption energies remain below the established targets for technological applications; however, their study in that sense contributes toward understanding the nature of the involved adsorption forces to optimize the design of porous materials for H_2 storage.

Acknowledgment. This study was partially supported by the Projects SEP-CONACyT 2007-61-541 and 82964, ICyTDF-PIFUTP08-158, DGAPA IN112109, and 23-06 IMPULSA. The authors acknowledge the access to the LNLS synchrotron radiation facility (Campinas, Brazil) to obtain information on the behavior of materials upon heating and then cooling.

Supporting Information Available: Structural and spectroscopic data, TG curves, and CO_2 and H_2 adsorption isotherms for all of the studied samples. This material is available free of charge via the Internet at http://pubs.acs.org.

(48) Reguera, E.; Rodríguez-Hernández, J.; Champi, A.; Duque, J. G.; Granado, E.; Rettori, C. *Z. Phys. Chem.* **2006**, *220*, 1609–1619.
(49) Arean, C. O.; Palomino, G. T.; Carayol, M. R. L. *Appl. Surf. Sci.* **2007**, *253*, 5701–5704.
(50) Georgiev, P. A.; Albinati, A.; Mojet, B. L.; Ollivier, J.; Eckert, J. *J. Am. Chem. Soc.* **2007**, *129*, 8086–8087.
(51) Serykh, A. I.; Kazansky, V. B. *Phys. Chem. Chem. Phys.* **2004**, *6*, 5250–5255.